This paper was awarded in the II International Competition (1993/94) "First Step to Nobel Prize in Physics" and published in the competition proceedings (*Acta Phys. Pol. A* **88** Supplement, S-77 (1995)). The paper is reproduced here due to kind agreement of the Editorial Board of "Acta Physica Polonica A".

COAXIAL PLASMA GUN IN THE HIGH DENSITY REGIME AND INJECTION INTO A HELICAL FIELD

S.F. Schaer

Centre de Recherches en Physique des Plasmas (CRPP) Association EURATOM Confédération Suisse, 21, Av. des Bains, 1007 Lausanne, Switzerland

Abstract

A modified coaxial plasma gun in the high density regime of 20–70 mT of He was investigated experimentally and theoretically. The injection of the plasma torus into a drift space was studied by diamagnetical diagnostics both with and without helical bias, where the inner electrode was continued into the drift space by an insulated central conductor. Quasi-tokamak geometry is obtained ($q \approx 3; I_\mathrm{i} \approx 1.2; \beta_\mathrm{p} \approx 0.7$). Mean speed of torus in drift space: 2.2 cm/μs, which is in excellent agreement with the MHD model derived. The theoretical considerations include: (1) acceleration phase, (2) ejection, (3) injection, (4) motion in the drift space, (5) tokamak stability. Discussion of: (1) general characteristics and phenomena, (2) second half-period breakdown with autopreionization, (3) prevention of transversal expansion by rarefaction waves of Mach 50 supersonic flow, (4) stability and homogeneity enhancement (factor 5), (5) agreement with model, (6) X-points and breakdown dependence, (7) velocity limitation, (8) thermal diffusion. The findings are, among other application domains, important for future designs of injectors for magnetic confinement, especially for spheromaks.

PACS numbers: 52.80.–s

1. Introduction

Plasma guns were first investigated by J. Marshall and H. Alfvén between 1958 and 1960 [1–4]. Most studies were done between 1960–65 [5–10]. Plasma guns were thoroughly investigated; however, a lot of questions remained unanswered, especially if the gun is operated in the high density regime. Thus the investigation of gun phenomena is still today a research task [11–14]. Plasma guns are used to inject plasma into all kinds of magnetic confinement devices, i.e. into conventional mirror machines [15], cusped traps [16], tandem mirrors [17], octupoles [18], tokamaks [19], stellarators [20], and spheromaks [21]. Furthermore, they are important to plasma dynamics research (MHD and kinetic) [22], dynamics of fast ionizing shock waves in MAST[1] devices [23], and for space propulsion [24].

[1]Magnetic annular shock tube = coaxial plasma gun (CPG).

Plasma centrifuges [25] are based on coaxial guns. Finally, they are used for deposition processes [26] and for REB[2] interaction studies [27]. A closely related field, i.e. dense plasma foci [28], has also become of considerable interest. It is thus of great interest and value to achieve a thorough understanding of plasma gun phenomena. This paper wants to make its contributions towards achieving that goal. Short publications of this work appeared in [39, 40].

2. Theoretical considerations

The model that one has to apply to a particular plasma gun is heavily dependent on the design parameters, i.e. capacitor bank characteristics, aspect ratio of the gun, whether or not the gun is operated with a gas puff, the kind of gas used, etc. Thus for the assumptions, approximations and computations, the design parameters have been introduced from Secs. 3 and 4.

2.1. Model for the acceleration phase

After breakdown which occurs at the gun-breech for lowest self-inductivity reasons, the generated plasma sheet is accelerated towards the muzzle by the magnetic field pressure of the discharge current supplying the plasma. In the high density regime, the sheet has to pull the rest gas, thus a fast shock wave with sufficient energy for partial ionization forms preceding to the sheet (Fig. 1). The classical snowplow model [29] is very well applicable

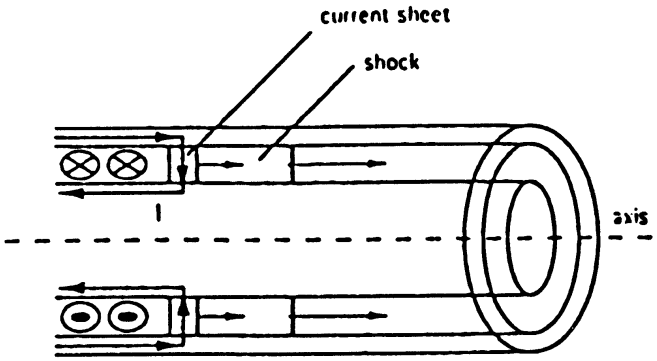

Fig. 1. Current sheet and shock region in the coaxial plasma gun.

to this gun, because (1) there is preionization, (2) the sheet speed < thermal speed, and (3) collisions between particles are important. The sheet is very homogeneous due to a clean breakdown and fast azimuthal exchange, since thermal speed < Alfvén speed. Wall friction due to ion drag occurs at much higher speeds than encountered in this experiment, thus it is neglected (especially for helium the drag is negligible, but not for argon [30]). The ion current is negligible too, since again the density is high, so that there are well enough ions in the central region hitting the cathode to strike out electrons. This is important because the electric field across the plasma is very small after breakdown, so that electrons are only able to leave the cathode through a collision interaction. According to the plasma parameters and previous papers, Maxwellian distribution is assumed for the electrons with a mean temperature of 10 eV. That value was confirmed by previous authors by means of magnetoacoustic oscillations and inference of plasma parameters from mapping procedures [6, 7, 31]. Since the design parameters of this gun are in the same range, the electron temperature was not measured again. 10 eV is well below the

[2]Relativistic electron beam.

Table I. Plasma parameters.

Electron temperature	10 eV
Mass density of the He rest gas (optimum)	1.1×10^{-5} kg m^{-3}
Mean free time	1.9 ns
Mean free path	4.3 mm
Degree of ionization (Saha)	$\approx 100\%$
Plasma conductivity for $I \perp B$	3.2×10^4 S
Max. magn. field of discharge current	0.4 T
Mean electron Larmor gyration freq. at max. of magn. field	15 GHz
Mean electron Larmor gyration radius	3.3×10^{-5} m
Hall parameter	174 ($\gg 1$)
Debye length	5.8×10^{-7} m
Number of particles in Debye sphere	1.34×10^3
Voltage across plasma at discharge current max.	25 V

occurrence of run-away electrons [32]. Table I gives the parameters of the plasma during acceleration (the design parameters have been introduced into the computations). For the mean free time, the mean free path, and the conductivity computation the Spitzer relations [33] have been used. A Laplace network analysis was carried out for the discharge current, but is not shown here. From the analysis it was seen that to assume a current of the form

$$I = I_0 \sin \omega t, \tag{1}$$

where I_0 is the amplitude of the ignition half-period, within which the plasma is ejected (in this case, only that very period is of interest), is very reasonable, since also $L_{\text{circuit}} \gg L_{\text{gun}}$, and $\mathrm{d}L_{\text{gun}}/\mathrm{d}z$ is very small, i.e. ω remains essentially constant. According to Table I the discharge current is fully thermalized. The transverse electron drift speed including the Larmor gyration correction factor is given by

$$v_{\text{d}} = \frac{I_0 \sin \omega t}{4\pi r n e \sqrt{2Dt}}, \tag{2}$$

$$D = \frac{1}{\mu_0 \sigma}, \quad \sigma = 14.86 \frac{\pi \varepsilon_0 (kT)^{3/2}}{Z m_{\text{e}}^{1/2} e^2 \ln \Lambda}, \quad \Lambda = \frac{12\pi (\varepsilon_0 kT)^{3/2}}{n^{1/2} e^3}. \tag{3, 4, 5}$$

The infinitesimal elements (concentric rings) are therefore treated as magneto-hydrodynamical elements of a fully thermalized discharge current. Compare with Figs. 2 and 3; from momentum considerations, it is readily found that

$$\frac{\mathrm{d}}{\mathrm{d}t} [M u_z] = I_0^2 \sin^2 \omega t \cos \alpha \frac{\mu_0 \Delta r}{4\pi r}, \tag{6}$$

$$\frac{\mathrm{d}}{\mathrm{d}t} [M u_r] = I_0^2 \sin^2 \omega t \sin \alpha \frac{\mu_0 \Delta r}{4\pi r}. \tag{7}$$

B has to be averaged over the sheet length because of ∇I_{axial}. The factors $\sin \alpha$ and $\cos \alpha$ appear because of $\nabla u_{z,\text{radial}}$ and because the discharge current is confined within the curved sheet. M is the total mass, i.e. the mass of the hot current sheet region expanding according to $(2Dt)^{1/2}$, and the snowplowed mass by the sheet. In the high density regime, snowplowing is both caused by collisions and by collisionless Coulomb turbulence, so that ξ is essentially 1; therefore it will not be written in the following formulae. From the shock

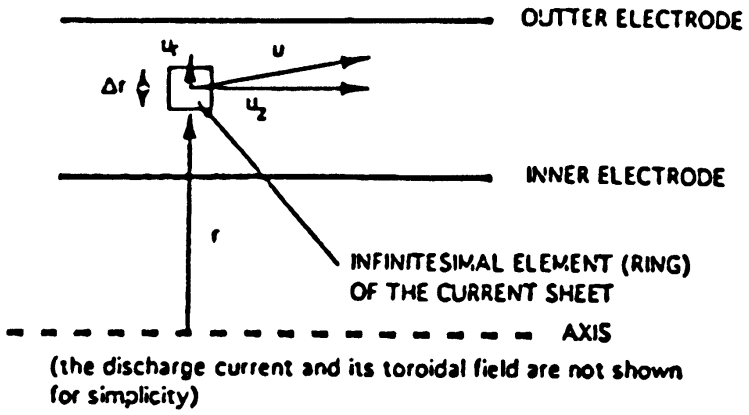

Fig. 2. Illustration of an infinitesimal current sheet element.

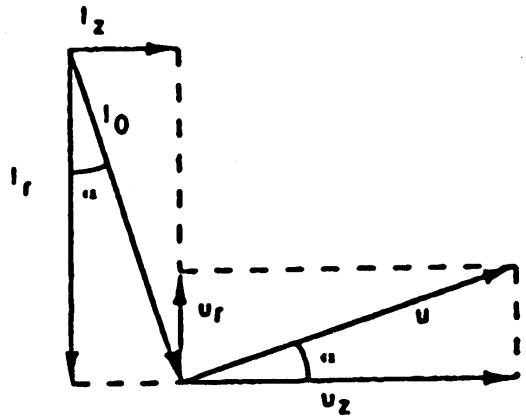

Fig. 3. Discharge current distribution geometry.

wave theory of Hugoniot–Rankine [34], where it is implemented that the Mach number $N_m \gg 1$:

$$\mu^2 = \frac{\gamma - 1}{\gamma + 1} = \frac{1}{f+1}, \quad u_\mathrm{s} = \frac{u_z}{1-\mu^2} = \frac{f+1}{f} u_z, \quad p_1 = \frac{f+1}{f} u_z^2 \rho_0. \qquad (8,\ 9,\ 10)$$

Upon calculating the total element mass as discussed above and performing a couple simple manipulations, (6, 7) turn into

$$M = 2\pi r \Delta r (1+f)\rho_0 \left(\sqrt{2Dt} + \frac{1}{f}\int_0^t u \mathrm{d}t \right), \qquad (11)$$

$$\frac{\mathrm{d}}{\mathrm{d}t}\left[r \frac{\mathrm{d}z}{\mathrm{d}t} \left(\sqrt{2Dt} + \frac{1}{f}\int_0^t u \mathrm{d}t \right) \right] = I_0^2 \sin^2 \omega t \cos\alpha \frac{\mu_0}{8\pi^2 r (1+f)\rho_0}, \qquad (12)$$

$$\frac{\mathrm{d}}{\mathrm{d}t}\left[\frac{\mathrm{d}(r^2)}{\mathrm{d}t} \left(\sqrt{2Dt} + \frac{1}{f}\int_0^t u \mathrm{d}t \right) \right] = I_0^2 \sin^2 \omega t \sin\alpha \frac{\mu_0}{4\pi^2 r (1+f)\rho_0}. \qquad (13)$$

The boundary conditions of the system (12, 13) are clear, for $t = 0$ they are: $\mathrm{d}z/\mathrm{d}t = 0$, $\mathrm{d}r/\mathrm{d}t = 0$, $z = 0$, $r = r_0$, $\cos\alpha = 1$, $\sin\alpha = 0$. Radial motion and electrode wall reflections[3] only have a small impact on the current sheet front and therefore on u_z. Disruptions or discontinuities in the sheet are quickly compensated with new ionized gas. However, the snowplowing is affected since it is no longer parallel to the axis. In the

[3]The impact is an amplification of the density gradient within the sheet.

following, axial snowplowing only will be assumed for simplicity, and a posteriori it will be seen that the error introduced is negligible. Thus $\mathrm{d}r/\mathrm{d}t$ is neglected, but (12, 13) used for numerical integration in order to obtain a mean value for $\cos\alpha$[4]. Then the system of (12, 13) reduces to

$$\frac{\mathrm{d}}{\mathrm{d}t}\left(\frac{\mathrm{d}z}{\mathrm{d}t}\sqrt{2Dt}+\frac{1\mathrm{d}(z^2)}{2f\mathrm{d}t}\right)=I_0^2\sin^2\omega t\cos\alpha\frac{\mu_0}{8\pi^2r^2(1+f)\rho_0}. \tag{14}$$

An approximated analytical solution can be obtained upon assuming $(2Dt)^{1/2}=\langle d\rangle$ to be constant, as previous authors have observed it [31]. The term with $\mathrm{d}(z^2)/\mathrm{d}t$ is dominant, so that diffusion only plays a minor role and could be neglected; the snowplowed shock mass is $\gg$ than the sheet mass. This is confirmed upon numerical integration of (14), both for constant and time-varying diffusion length. For completeness however, $\langle d\rangle$ is included in the following formulae[5]. The equation is then easily solved by separation of variables and analytical solutions for z and u_z dependent on time and the parameters are obtained

$$K=\frac{\mu_0\cos\alpha}{8\pi^2r^2(1+f)\rho_0}, \tag{15}$$

$$z=f\left(-\langle d\rangle+\sqrt{\langle d\rangle^2+\frac{KI_0^2}{2f\omega^2}(\omega^2t^2-\sin^2\omega t)}\right), \tag{16}$$

$$u_z=\frac{KI_0^2(\omega t-\sin\omega t\cos\omega t)}{2\omega\sqrt{\langle d\rangle^2+\frac{KI_0^2}{2f\omega^2}(\omega^2t^2-\sin^2\omega t)}}. \tag{17}$$

[6] found similar formulae, except K was different since no snowplowing was included, because the gun was operated in the "slug" gas puff mode with acceleration of plasma into vacuum. Furthermore, the equation did not include $\langle d\rangle$, thus the form is slightly different; the double integration of $\sin^2\omega t$ however remains the same as in this case. From the numerical integration the mean value of $\cos\alpha$[6] is computed to $\approx 1/2$ (the sheet becomes conical). Table II gives some sample values for different times at the mean radius of 4 cm, computed according to (16, 17), where the optimum parameters have been introduced from Sec. 4; $\langle d\rangle$ is computed to have an average value of 1 cm according to Table I and (4). The mean radius of 4 cm was chosen, because the toroidal plasma current density has a maximum there and the toroidal current is what was measured by the diamagnetical probes[7].

If $\langle d\rangle$ were set zero in (16, 17), the relative error of u_z within the relevant times of Table II would be less than 2%. Therefore, thermal diffusion does not have to be considered for the relevant times during the acceleration phase in this experiment and most other plasma guns, where the ejection time might be even shorter. Figures 4 and 5 show the graphs of $z(t)$ and $u_z(t)$; $z(t)$ is very quickly close to be linear, thus a plasma gun in the high density regime will exhibit velocity limitation, as observed by previous authors [35]; (17) is a simple explanation. If the functions are evaluated over more than one discharge current period, damping should be included. However, this only gives smaller

[4]The author does not want to focus in on the numerical integration, because the following analytical formulae give the same values for u_z with negligible relative error.

[5]In Sec. 2.4 $\langle d\rangle$ will have to be included in the consideration. Generally, for larger t, $\langle d\rangle$ has to be included, so that it is also included in the following formulae.

[6]This factor too was assumed to be constant during acceleration.

[7]The two INOX-cylindrical electrodes of the discharge chamber have the radii 3 cm and 5 cm.

Table II. Sample values of z and u_z at $r = 4$ cm for different t.

t (in μs)	z (in cm)	u_z (in cm/μs)
1	0.25	0.9
2	2.5	3.5
3	6.6	4.5
4	11	4.2
5	15	3.5

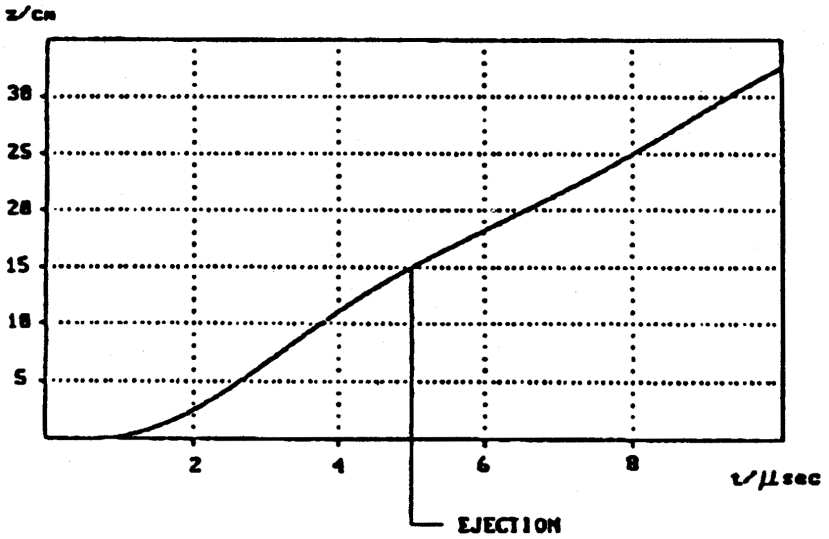

Fig. 4. Graph of $z(t)$; from $t = 2$ μs on z increases almost linearly with t. Ejection is at $z = 15$ cm, which is the length of the gun. Then $t = 5$ μs. Of course, the graph is no longer valid for $t > 5$ μs for this gun, but to illustrate that the curve is almost linear this section was included too. It would hold for a gun with longer electrodes, i.e. larger ejection time.

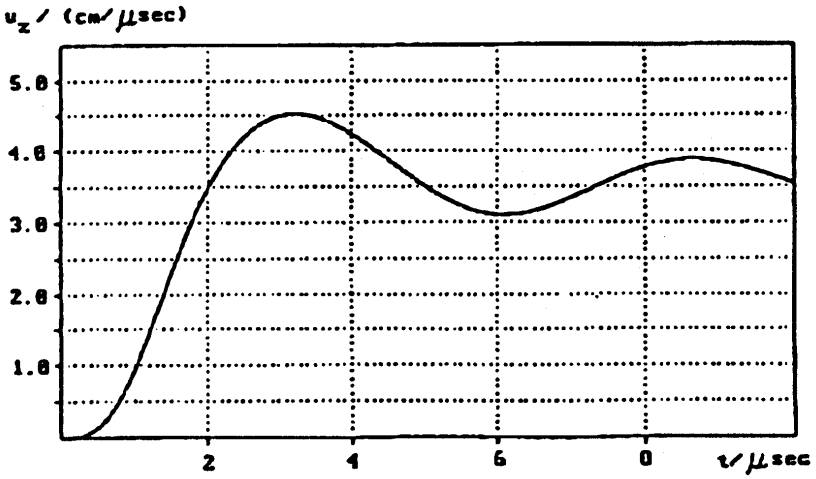

Fig. 5. Graph of $u_z(t)$; it is seen that the maximum speed of 4.5 cm/μs is reached at approximately $t = 3.2$ μs. At ejection $u_z = 3.5$ cm/μs.

values of the functions at larger t, the limitation in the oscillatory case is not affected. Further periods are of no interest in this experiment, since the sheet is ejected within the first half-period. Figure 6 shows the motion of the current sheet during acceleration computed according to (16, 17). This is in agreement with SEM (scanning electron

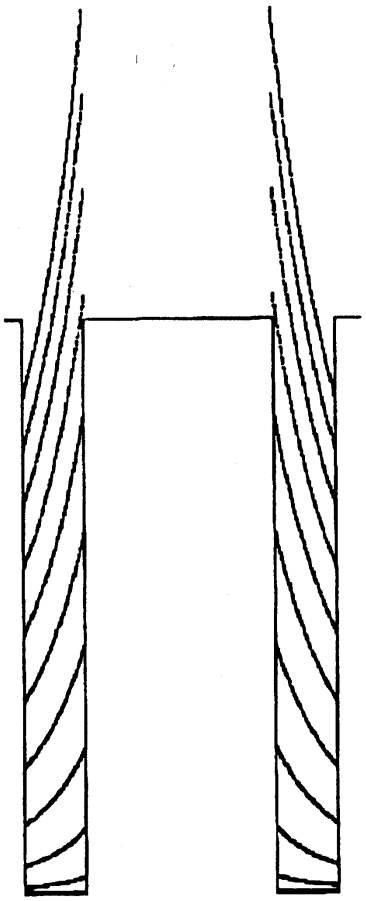

Fig. 6. Motion of the plasmoid in the acceleration phase computed according to (16, 17).

microscopy) image converter camera picture of a previous author [5, 7, 11]. The front surface is hyperbolical. The plasma tori that are ejected are thus elongated. Of course, this model cannot account for all effects. For example, the spin of the torus was neglected, thermal diffusion taken constant, no electron nor ion temperature gradient was included, axial snowplowing only was considered, electrode material ablation and other plasma-wall interactions neglected, etc. But to account for everything is widely beyond the scope of this work and the necessity of having to include them for experimental testing of the model (16, 17). In Sec. 4 it will be seen that the values of Table II are in very good agreement with experimental data.

2.2. Ejection phase at the muzzle of the gun

When the plasmoid reaches the muzzle, it is ejected from the gun due to high u_z (Fig. 7). A toroidal current is induced into it through flux conservation of the permanent, radial magnetic field. It is not exactly known when the discharge current through the sheet is interrupted. One might expect that the current continues to flow as an arc between the edges of the two cylinders, until finally it is interrupted. But experimental data suggest that the gun remains short circuited at the muzzle, so that the sheet can exit freely. The central part of the sheet in the drift space is therefore heavily dependent on the aspect ratio of the gun. For small aspect ratio, it will be flattened [11], but for a large one very conical [7]. (18) gives the toroidal current induced in the plasma, where for the flux conservation it has been assumed that the flux in the drift space is enclosed totally within the outer aluminum cage (Sec. 3). Ξ is a geometry dependent factor found

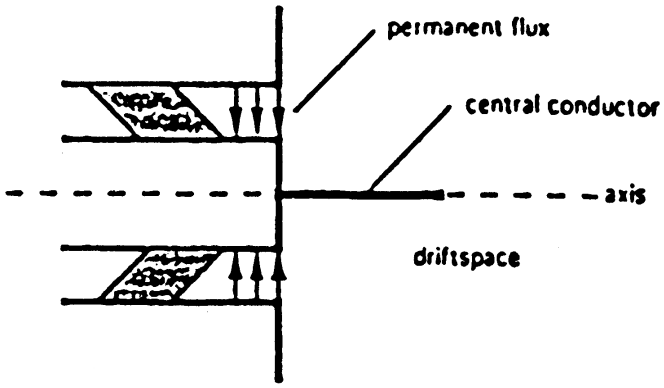

Fig. 7. Current sheet at the muzzle of the gun.

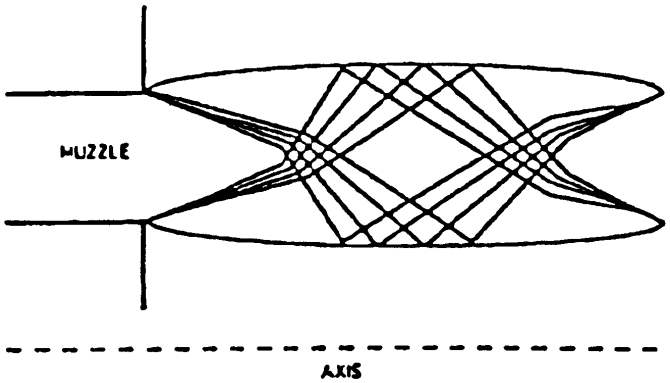

Fig. 8. Simplified rarefaction-wave pattern at the muzzle preventing significant transverse expansion. The intercepting shock wave pattern was simplified.

by surface integration, whereas κ has to be assumed (1 in our case).

$$I_{\mathrm{p}} = \frac{\kappa\Phi}{\mu_0 \Xi}, \qquad \Xi = \left[b - \frac{2}{3}a + R\left(\frac{1}{2} + \ln\frac{b}{a}\right)\right]. \tag{18, 19}$$

This current magnetizes the plasma producing a confining poloidal field, which drastically aids the stability of the ejected plasma rings. These elongated rings really do have enough mass to be considered as such, since thermal diffusion should not be forgotten. The current is then distributed over the whole torus cross-section with a gradient. At the ejection, a highly supersonic flow of Mach 50 enters a region of lower pressure. There are two edges at the muzzle, one of the inner and one of the outer cylindrical electrode. Figure 8 shows the rarefaction wave pattern that forms [34]. It is readily seen that this prevents transverse expansion at first, therefore enhancing stability. The effect of magnetic field components in the supersonic flow pattern was neglected.

2.3. Drift space phase without axial bias field — toroidal bias

Without axial bias field means with toroidal bias only (in this experiment), since the helical bias will be generated by a superposed axial field to the toroidal field. The phenomena at ejection are very complex: Bohm diffusion, curvature drift, rarefaction wave pattern, rotation around the axis, poloidal field envelopping, X-point occurrence, etc. A simple approach from momentum conservation is made in the following, where radial motion and transverse expansion are neglected to begin with (rarefaction waves

prevent transverse expansion). From momentum conservation

$$u_0\left(\sqrt{2Dt_0}+\frac{l_{\rm gun}}{f}\right)=\frac{1}{2f}\frac{{\rm d}(z^2)}{{\rm d}t}+\left[\sqrt{2D(t+t_0)}+\frac{l_{\rm gun}}{f}\right]\frac{{\rm d}z}{{\rm d}t}, \tag{20}$$

$$z=f\left[-A+\sqrt{A\left(A+\frac{2u_0t}{f}\right)}\right], \tag{21}$$

$$u_z=\frac{u_0\sqrt{A}}{\sqrt{A+\frac{2u_0t}{f}}}, \tag{22}$$

where $A=(\langle d\rangle+l_{\rm gun}/f)$; t and z are set zero at the time of ejection. The same approximations have been made to solve (20) as to solve (16). $\langle d\rangle$ has to be considered in this case at larger t, otherwise the induced error is of the order of 8%. Table III shows some sample values for u_z in the drift space, and Figs. 9 and 10 show the graphs of $z(t)$ and $u_z(t)$ for the plasmoid in the drift space. The speed that is finally measured in the form of a time delay is that at the mean radius (4 cm), since the toroidal plasma current density has got a maximum there.

Table III. Sample values of u_z in the drift space for different t ($t=0$ at ejection) at $r=4$ cm.

t (in μs)	u_z (in cm/μs)
1	3.0
2	2.6
3	2.4
4	2.2
5	2.0
6	1.9

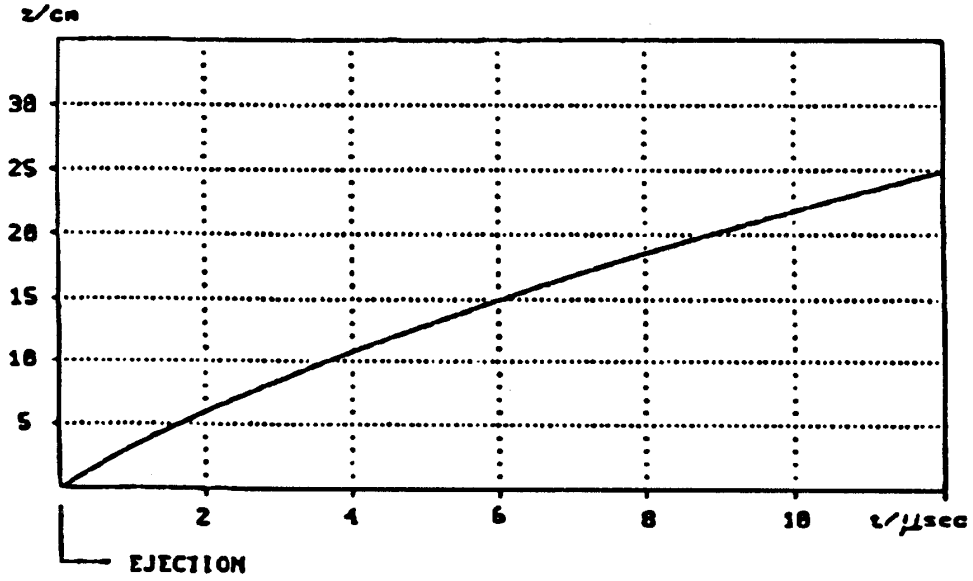

Fig. 9. Same as Fig. 4, but for the drift space phase. The function is still close to be linear within the relevant times. Here, $t=0$ and $z=0$ at ejection.

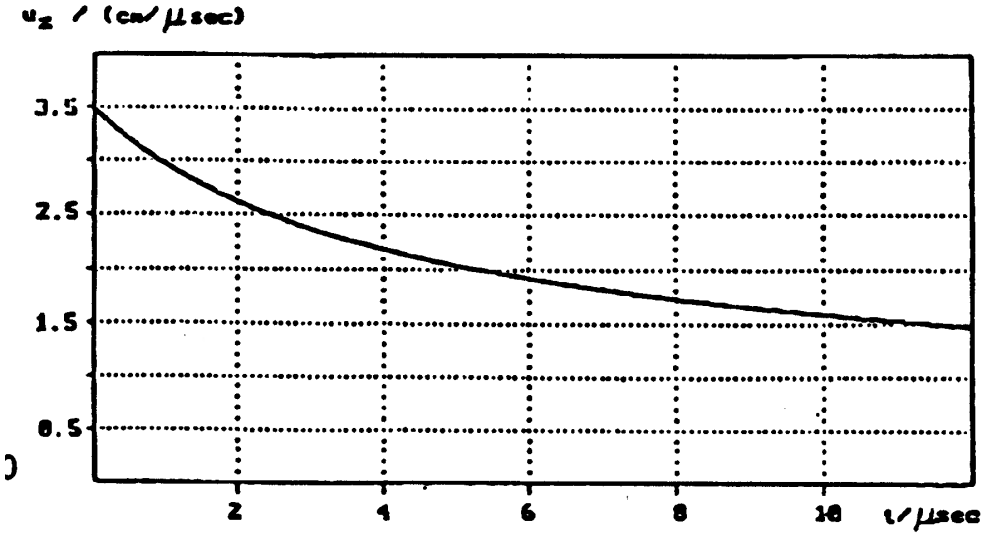

Fig. 10. Same as Fig. 5, with the same modification as in Fig. 9.

2.4. Drift space phase with axial bias field — helical bias

The magnetized elongated torus is injected into a helical bias field, produced by the toroidal field of the leakage current in the central conductor and the coil-generated field, which can be considered as quasi-tokamak field geometry (Fig. 11). The plasmoid moves

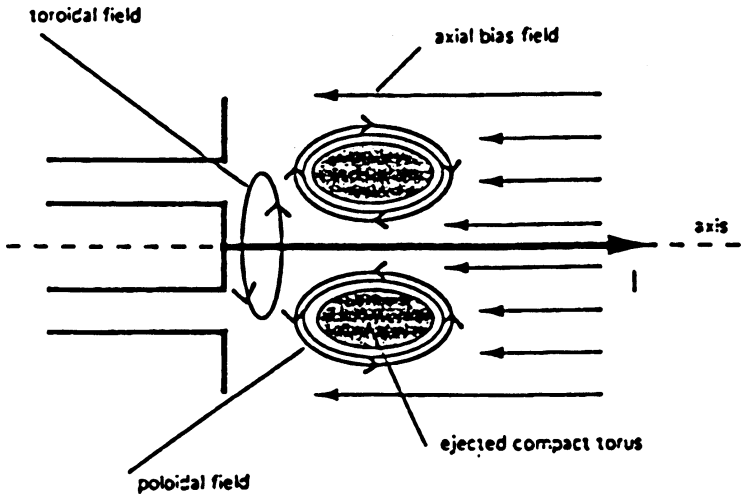

Fig. 11. Ejected current-carrying (elongated) plasma torus in the drift space.

as in Sec. 2.3, but it is slowed down slightly by the magnetic pressure gradient of the bias field. Recent findings at the spheromak SPHEX with an independent central iron rod [21] show an enhancement of torus stability. In this work it was tried whether it was possible to use an elongated central electrode (as described) instead of an independent rod in order to achieve better gun operation and enhanced stability after injection. The stability enhancement is treated with an approach from tokamak physics. The necessary axial field strength has been computed according to Shafranov's formula (23) [36, 37]:

$$B_{\mathrm{a}} = -\frac{\mu_0 I_{\mathrm{p}}}{4\pi R}\left(\ln\frac{8R}{a} + \Gamma - \frac{1}{2}\right), \qquad \Gamma = \beta_{\mathrm{p}} + \frac{I_{\mathrm{i}}}{2} - 1 \qquad (23,\ 24)$$

The definitions used for β_p, I_i, and q are

$$\beta_\mathrm{p} = 1 + \frac{1}{(aB_{\theta,a})^2}\int_0^a \frac{\mathrm{d}B_\Phi^2}{\mathrm{d}r} r^2 \mathrm{d}r \approx 0.7, \tag{25}$$

$$I_\mathrm{i} = \frac{\int_0^a (B_{\theta_0}^2/2\mu_0) 2\pi r \mathrm{d}r}{(B_{\theta_{0,a}}^2/2\mu_0)\pi a^2} \approx 1.2, \tag{26}$$

$$q = \frac{1}{2\pi}\oint \frac{1}{R}\frac{B_\Phi}{B_\theta}\mathrm{d}s \approx \frac{aB_\Phi}{RB_\theta} \approx 3. \tag{27}$$

The numerical values are given for the optimum parameters from Sec. 4. The field profile inside the torus was taken to have a squared parabolical form.

3. Experimental apparatus

Due to the unique design of the gun, some effects not anticipated were found. These are discussed at the beginning of Sec. 4, here, only the apparatus itself is presented as it has been planned.

3.1. Modified coaxial gun and drift space

Figure 12 depicts the heart piece of the apparatus. The discharge chamber lies between $r = 3$ cm and $r = 5$ cm, having a total acceleration length of 15 cm. The electrode material is INOX, the insulator teflon. Actually, the discharge is short circuited, by the central conductor (insulated from the drift space by a thin pyrex tube), the copper cross, the bottom plate, and the outer aluminum cage. But due to the high self-inductance of that circuit, the discharge takes place anyway. The leakage current through the central conductor generates the toroidal field necessary for the helical bias, together with the axial field coil. Due to the central conductor, the large discharge current is not interrupted, when the plasmoid is ejected. In previous experiments, the current has been observed to continue as a helical pinch, if this is not provided [7]. The pyrex tube of the drift space has an inner radius of 8.5 cm and a total length of 48 cm. The diagnostics and the axial field coil are held by a hexagonal cage, embedded between the aluminum cage and the pyrex tube. The radial field at the muzzle of the gun is generated by assembled permanent-magnet cubes, lying on top of the inner electrode. The flux is guided to the muzzle through the massive iron plates (not in axial symmetry) and the central iron core. The permanent field strength reached in this manner is 0.2 T. The leakage flux is negligible. Unique are the central conductor and the outer aluminum cage. At the gun breech, an INOX ring with a sharp edge has been mounted on the inner electrode to stimulate ignition. The polarity has been chosen negative to begin with. In Sec. 4 it is explained why the polarity was not changed although it was found that a positive inner electrode stimulates immediate breakdown. For more details, the reader is referred to the legend of Fig. 12. Note that this design is much less complicated than previous guns.

3.2. Vacuum system

Helium was chosen as the working gas; the pressure was varied as parameter between 20 mTr and 70 mTr. For this pressure range, a common rotary pump is adequate. The vacuum chamber is evacuated well below 1 mTr, before helium is admitted. This experiment does not use a fast-acting valve as a gas puff, thus the helium is admitted through a manual valve. This allows the acceleration of a considerable amount of mass. After a period of preliminary tests, it was found that the discharge chamber, especially the teflon

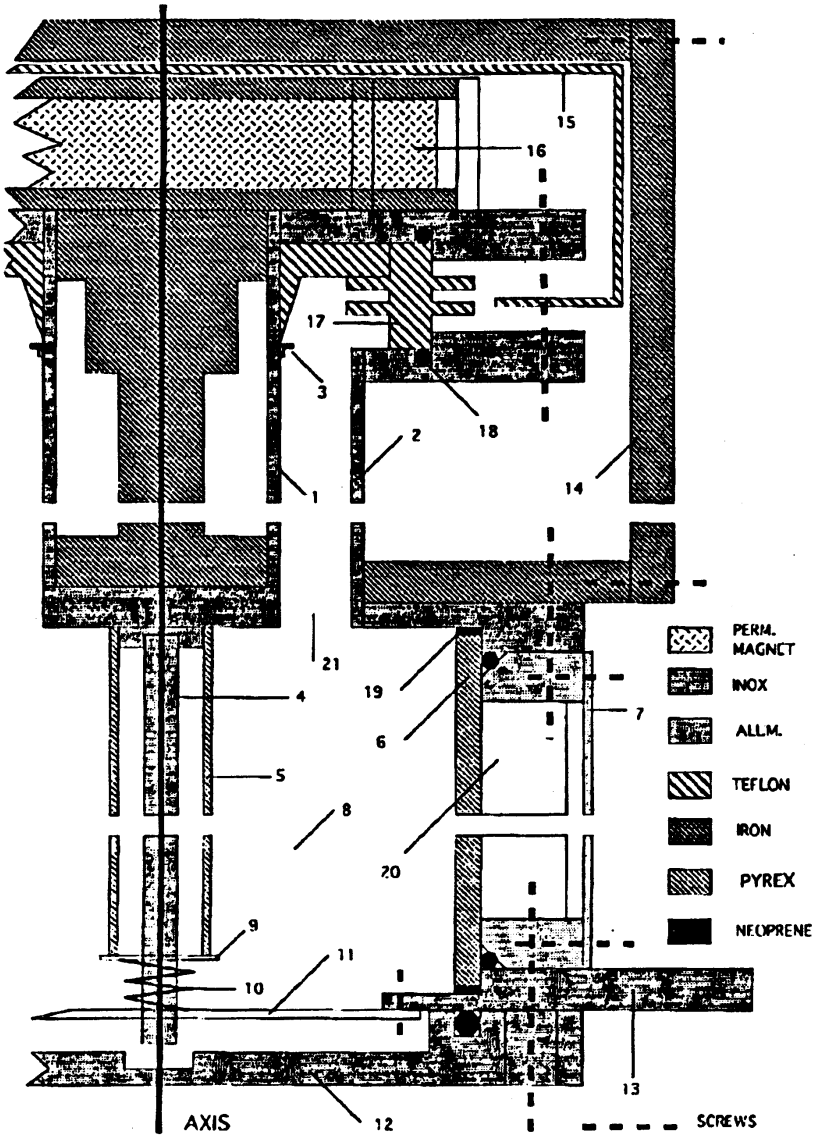

Fig. 12. Heart piece of the apparatus: 1 — inner electrode, 2 — outer electrode, 3 — ignition aid (INOX disc), 4 — central conductor, 5 — thin pyrex tube insulating the central conductor, 6 — pyrex tube of the drift space, 7 — aluminum cage, 8 — drift space, 9 — teflon disc, 10 — coil spring, 11 — copper cross, together with 9, 10 fixing 5 elastically, 12 — removable bottom plate, 13 — fixed bottom plate, 14 — permanent flux guide (not constructed in axial symmetry), 15 — teflon insulation layer, 16 — permanent magnet, 17 — teflon ring insulating the two discharge electrodes, 18 — O-ring, 19 — neoprene ring for elastic fixation of 6, 20 — hexagonal cage fixing axial field coil and the probes of the diagnostics, 21 — muzzle.

insulator, became too dirty due to the oil steam coming from the pump and other degassing pollutants like water vapor. Therefore, a liquid nitrogen cryotrap has been added and the problem was reduced to a very well acceptable level.

3.3. Main and axial field coil discharge system

The triggering is performed by the same chain of pulse amplifiers for both discharges. A manual switch triggers a TTL time base unit with a resolution of 1 μs, from where everything else is triggered, i.e. discharges, oscilloscopes, etc. The timed pulse for each discharge is amplified from -5 V to $+300$ V, then from $+300$ V to -5 kV by a thyratron

pulser. That pulse is then coupled into a diode safety electronic by a HV coupling-transformer. Finally the ignitron is fired discharging the capacitors. The data given below have been calculated using transient Laplace network analysis, and are in agreement with experimental data.

3.3.1. Main discharge

The potential on a 13.7 μF low-inductivity capacitor is varied between 9 kV and 15 kV for the different shots. For 15 kV, the charging time is approximately 3 min. The discharge current has the form of a damped sinusoid, with $\tau_{\text{plasma}} = 15$ μs and $f_{\text{plasma}} = 200$ kHz when a plasma is ignited, and $\tau_{\text{central}} = 55$ $\mu\text{s}/f_{\text{central}} = 100$ kHz when the current flows through the central conductor. Originally, the circuit was intended to give a plasma discharge current of 100 kA, but due to second half-period breakdown discussed in Sec. 4, the maximum plasma discharge current is 86 kA. To keep the inductivity of the circuit low, the energy is transported from the coaxial capacitor to the gun by a low-inductivity slab line.

3.3.2. Axial field coil discharge

Two electrolytic capacitors having a total capacity of 6200 μF are charged to a potential of 50 V to 400 V, which is varied as a parameter. The polarity of the field generated by a coil of 25 turns can be changed. Coil currents reached are between 500 A and 4000 A, according to the discharge potential varied as parameter. The discharge itself is aperiodically damped by means of a flywheel diode, where $t_{\text{rise}} = 0.7$ ms and $\tau = 2$ ms. The charging time is 4 min for 400 V. The maximum field strength in the middle of the coil is 0.26 T.

3.4. Diagnostics

The discharge currents are measured by Rogowski coils. For plasma diagnostics, an array of 9 diamagnetical probes held by the hexagonal cage around the quartz tube is used. These probes are at a certain distance apart from each other; the time delay is measured and thus the velocity and position obtained. The pulses also allow the computation of the toroidal current, elongation, electron temperature, q- and β_{p} values, density profile, lifetime, and so on. Figure 13 shows the array of probes and one probe in detail. The pulse

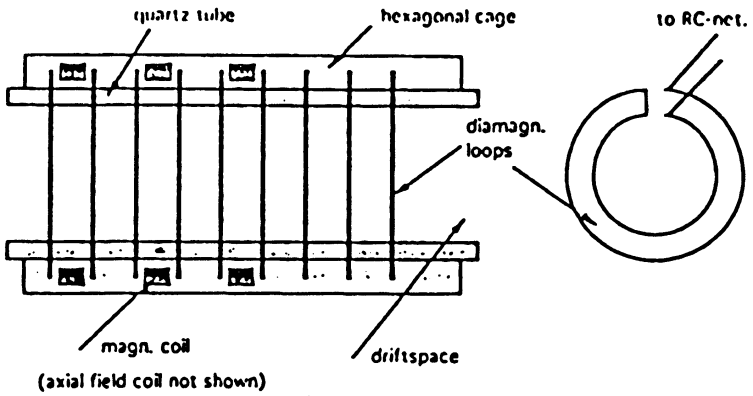

Fig. 13. Array of probes and one diamagnetical probe consisting of two nested loops in detail.

computations shall not be given here for space reasons. Figure 13 also shows 3 planes with 3 magnetical coils each. With that second array the uniformity of the toroidal current can very easily be measured. Instabilities up to $n = 3$ are possible to be detected.

4. Results

This section presents the experimental results. The results of the theoretical considerations have already been shown in Sec. 2, here it remains only to be shown that there is a very good agreement between the model and experimental data. To give a general impression, the pulses were highly reproducible despite the fact that the high density regime usually is very problematic.

4.1. Effects of electrode polarity: second half-period breakdown

This consideration starts at the time where the ignitron of the main discharge has been fired. The energy is delivered to the gun, the central cylindrical electrode having negative polarity. The inductivity of the short-circuit through the central conductor and the aluminum cage is much higher (4 times) than the discharge inductivity, so that one expects a breakdown. There is, however, an electron transit time effect. The electric field between the electrodes is still high, so that electrons can leave the central electrode. Now, the magnetic field of the current flowing through the central electrode (because the discharge current starts to flow) exerts a force on the electrons deflecting them in the axial direction (also, the rest gas is not preionized at that time point and the current not thermalized). That field is strong enough, so that the electrons cannot reach the outer, positive cylindrical electrode. Thus breakdown does not occur, and the current flows through the central conductor. But when the second half-period of the potential is reached, i.e. the outer cylinder is negative and the inner positive, electrons leave the outer cylinder and first are in a region of weaker toroidal magnetic field[8]. They have gained enough transverse velocity when entering the strong field region close to the inner cylinder, thus they can reach it and breakdown occurs. This is also enhanced by the preionization taking place on the first breakdown effort. Without a central conductor continuation, breakdown has to take place on the first half-period. But the polarity should still be negative to begin with in the central conductor operation mode, because autopreionization is very conveniently performed, resulting in very homogeneous, clean breakdowns on the second half-period. After thermalization of the discharge current, the phenomenon is expected to vanish, as it has been observed. Note that the central conductor does not lose its original purpose to generate a toroidal field in the drift space. When the plasma is ignited, the current in the central conductor circuit loop decays due to the high inductivity with $\tau = 55\ \mu$s, but the plasma is ejected within 3 μs to 4 μs, so that the toroidal field is still well maintained! Figure 14 shows a typical oscillogram for the total discharge current and the current through the central conductor. Note that the gun remains short circuited after breakdown. Through which circuit loop the current flows are easily distinguishable by the different resonant frequencies as discussed in Sec. 3.3; those were determined by means of transient Laplace network analysis.

4.2. Sensitivity of the breakdown to magnetic field components

This problem was first encountered when the operation of the axial field coil was started. Whenever there was a helical bias instead of a toroidal, no signal was measured by the diamagnetical probes. This can only suggest one thing: there is no toroidal current leaving the gun. It was found that this is due to a stable electron orbit effect at the muzzle of the gun. A complicated field geometry exists there. First, there is the radial field. But this alone cannot be the cause, because if this is the only field, the gun works fine. It must

[8]The breakdown occurs a little after the current goes through zero, so that there is a toroidal magnetic field.

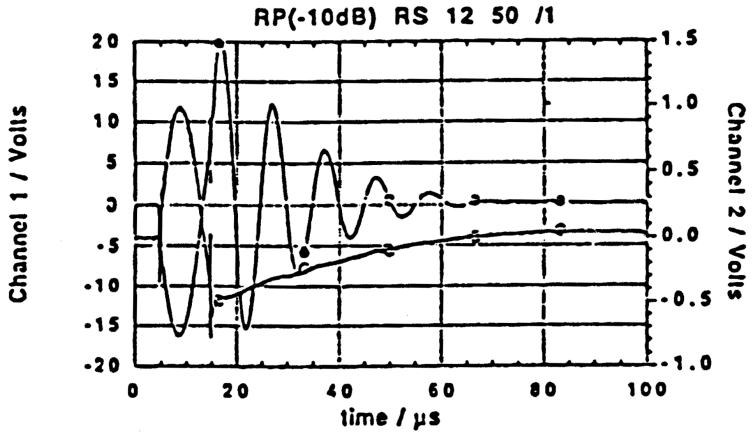

Fig. 14. Typical oscillogram for the discharge current (channel 1) and the current in the central conductor (channel 2). Channel 1: 4.3 kA/V, channel 2: 2.5 kA/V. The vertical spike at $t = 15$ μs indicates breakdown. The first half-period is longer since the discharge current flows through the central conductor loop, which has a much higher inductivity. • channel 1, ∘ channel 2.

thus be the axial field component of the coil that causes the problem. With an axial bias in that region, a quasi-magnetron geometry is obtained. Thus Brillouin clouds can form [38]. Stable electron orbits are greatly enhanced by that and the complex field geometry (stable orbit in X-point, etc.). Breakdown then occurs at the muzzle of the gun, and it is clear that no toroidal current will be measured by the diamagnetical probes. In order to get rid of that problem, a second, much shorter coil with 6 turns having a larger radius than the main coil has been added, as it is shown in Fig. 15. The second coil has opposite

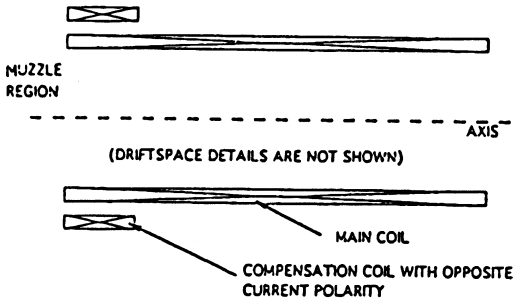

Fig. 15. Axial field coil with opposite current polarity compensation coil.

current polarity, and has been computed in such a manner that axial field components cancel out in the very region of the muzzle. The axial and radial components of the field, into which the plasmoid is injected, are shown in Fig. 16a and b. It must not be forgotten that those are twisted into a helix by the toroidal field of the central conductor. After having added that second coil, the gun worked just fine, so that the injection could be studied. This sensitivity of the breakdown to axial field components is also of importance to other guns, which are operated with axial bias in the discharge chamber region. Then, the breakdown region is no longer exactly defined, so that operation problems may arise. Therefore the author suggests to operate a coaxial plasma gun without axial components in the discharge chamber region unless the gun is operated in the "slug" mode. Axial components however are needed in the drift space region as the third necessary field for tokamak equilibrium, i.e. there will always be a complicated field geometry in the muzzle region which has to be assessed. The present compensation coil worked fine, except when

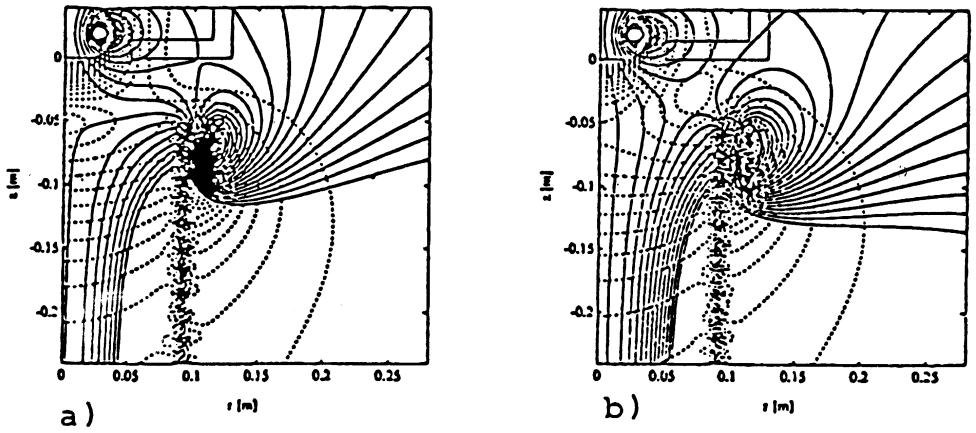

Fig. 16. Axial and radial components of the magnetic field, into which the plasmoid is injected. This geometry is actually twisted into a helix by the azimuthal components of the field. In the case of +4000 A (a) the gun worked fine, but for opposite field polarity (−4000 A) (b) in order to achieve flux amplification no toroidal current was measured. The bad breakdown for the latter situation is also influenced by the clearly visible X-point (−4000 A). The permanent field was represented with a current carrying loop. Not all field lines are shown for clarity.

"flux-amplification" with reversed field was tried. Then the X-point causes problems (Fig. 16b).

4.3. Results of plasma diagnostics with toroidal bias field

The optimum parameters within the range of variation are for this case: a discharge potential of 13 kV, and a pressure of 50 mTr, which has been computed to be the optimum. The pulses obtained were very highly reproducible, only unsignificant noise levels made up the vanishing difference. Consider Figs. 17a–f. In Fig. 17 (data are given in each figure's legend) it is clearly visible that the plasmoid with the toroidal current moves down the drift space. The pulse becomes smaller since the current decays, and due to ∇u_z, the pulse widens because the plasmoid is stretched. The current decay leads to a larger q value and therefore generally to higher stability. Figures 17b–f show the same, but the signals can be viewed much clearlier. Figure 17b indicates a time delay of 2 μs between two subsequent probes. Since the probes are spaced 4.8 cm apart from each other, the mean velocity is 2.4 cm/μs (the error introduced in the measurement is of the order of 3–6%; for convenience, this is not rewritten each time in the following). To compare: the MHD-model from Sec. 2 predicts a velocity of 2.6 cm/μs (compare with Table III)! The time delay between the second (D2) and the third (D3) diamagnetical probe is measured to 2.5 μs, thus $u_z = 1.9$ cm/μs. Again, the model predicts 2.1 cm/μs! This is really a very good agreement with the experiment. From Fig. 17 it is clear that the toroidal current lasts for at least 12 μs; which is rather long. The toroidal plasma current is computed from the extreme value of the pulse. For this probe design it is 2.13 kA/V. Thus the current in the torus is 6.4 kA when passing the first probe, but then it decays rapidly, i.e. β_p increases accordingly. The electron temperature drops to about 5 eV during the flight. It is found that the torus has a length of about 8 cm, which changes slightly as it propagates down the drift space[9]. The torus is very compact, as

[9]These calculations are not shown, since they are only of technical nature. For the same reason, the Laplace network analysis is not shown for the discharge current, the axial field coil discharge, or for the diamagnetical probe signal.

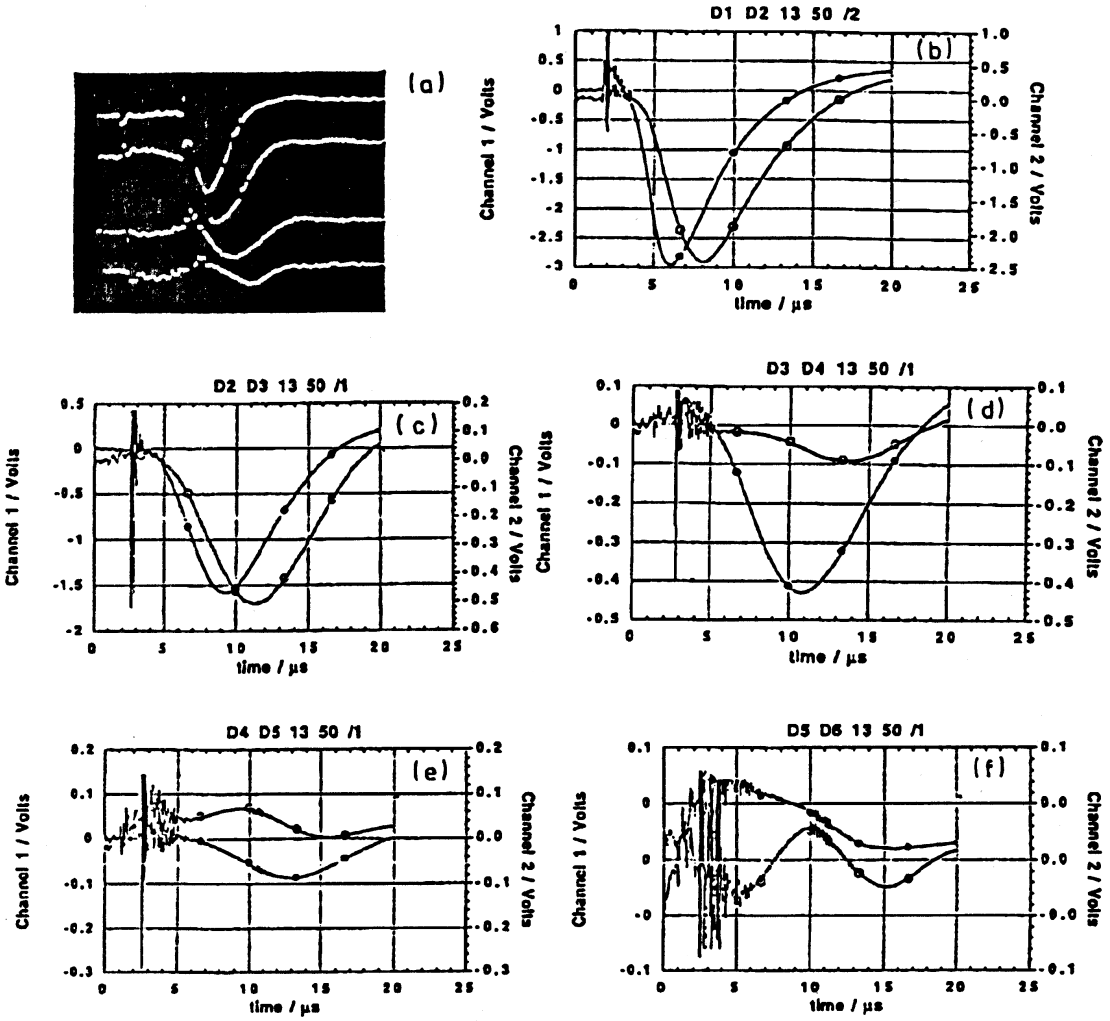

Fig. 17. (a) The movement of the torus in the drift space can easily be viewed in this picture from the oscilloscope. From top trace to bottom trace: D1 (2 V/div), D2 (2 V/div), D3 (1 V/div), D4 (0.5 V/div), where D means diamagnetical probe and the higher the index the further away the probe is from the muzzle. 5 μs/div, $p = 50$ mTr, 13 kV discharge potential; (b) The same parameters as in (a) — channel 1: D1, channel 2: D2, • channel 1, ∘ channel 2; (c–f) — analogously.

in a spheromak. According to the pulse shape, the toroidal current maximum is about in the middle of the whole pulse, i.e. in the middle of the conical shape if viewed from front to back, corresponding to $r \approx 4$ cm at ejection, as it has been introduced in Sec. 2. Therefore, the exiting plasmoid has two characteristics: on one hand, there is the conical sheet, but on the other hand, there really is a torus (about in the middle from front to back of the sheet). The magnetical diagnostics confirmed a very homogeneous toroidal current, because signals from the 3 coils per plane were identical. No n instabilities were observed, the decay of the current is very continuous and does not happen abruptly. No oscillatory instability occurred. Transverse expansion did indeed not take place, due to the rarefaction wave pattern discussed in Sec. 2.

4.4. Results of plasma diagnostics with helical bias field

A helical bias combined with the poloidal field of the toroidal current results in a quasi-tokamak field geometry. For this particular design, the optimum parameters within

the range of variation are: 13 kV/50 mTr/1000 A coil current, thus $B_{\max} = 0.065$ T, $I_{\rm i} \approx 1.2$, $\beta_{\rm p} \approx 0.7$, and $q \approx 3$. This is about three times less than the equilibrium field computed according to Shafranov's formula. The explanation will be given later on, since it is combined with some other effect. Again, the pulses obtained were highly reproducible. The speed of the sheet in the drift space is only insignificantly affected by the magnetic field. The geometry of the field, into which the torus is injected with $\beta = 0.7$, has been shown in Fig. 16. Figure 18 shows what is expected to happen to the plasmoid: the penetration into the stronger helical field region causes the toroidal current to decrease more rapidly. Figure 19 is the same series as Figs. 17 expect that

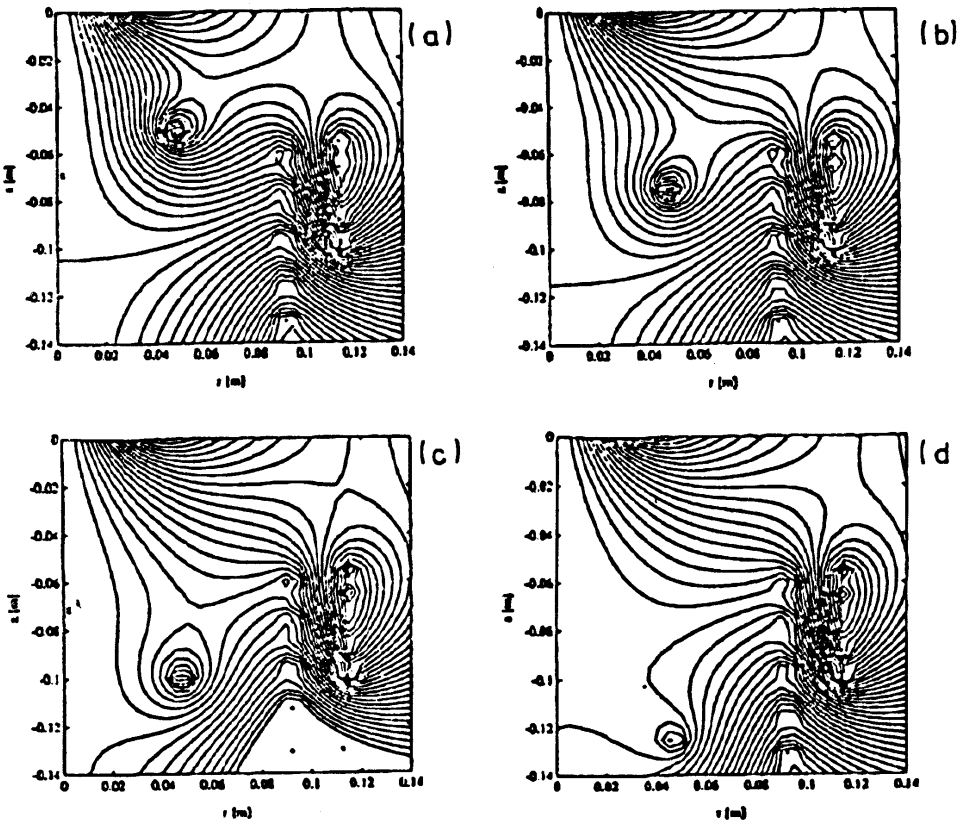

Fig. 18. (a) — Radial and axial field components after injection. The moving plasma torus is approximated with a current carrying loop. For this figure, the axial coil discharge current was 1000 A and the current in the ring 5000 A with opposite polarity. Note that this is only a model. Behind the plasma, an X-point occurs. The positions of the turns of the coils are clearly visible. The muzzle is at $z = 0$ between $r = 3$ cm and $r = 5$ cm. The axis is at $r = 0$. (b)–(d) — continued.

now, the discussed field geometry exists. Consider Fig. 19 a; the first 15 μs are noise, then, there is a short positive pulse followed by a wider, negative one. This includes a neat diamagnetical measurement of the preceding fast shock wave. When the shock front reaches the muzzle of the gun, helical current discharges take place into the drift space[10]. Those are caused by the ionizing front being ejected, forming a rarefaction wave pattern.

[10]A helical current discharge is encountered when helical current exits from the flat end of the inner cylindrical electrode into the drift space (not the same as the ejected plasmoid or the central conductor leakage current). The experimental setup is in such a way that the probes must give a positive pulse for a helical current discharge, and a negative one for the propagating toroidal plasma current, because the current polarities are opposite.

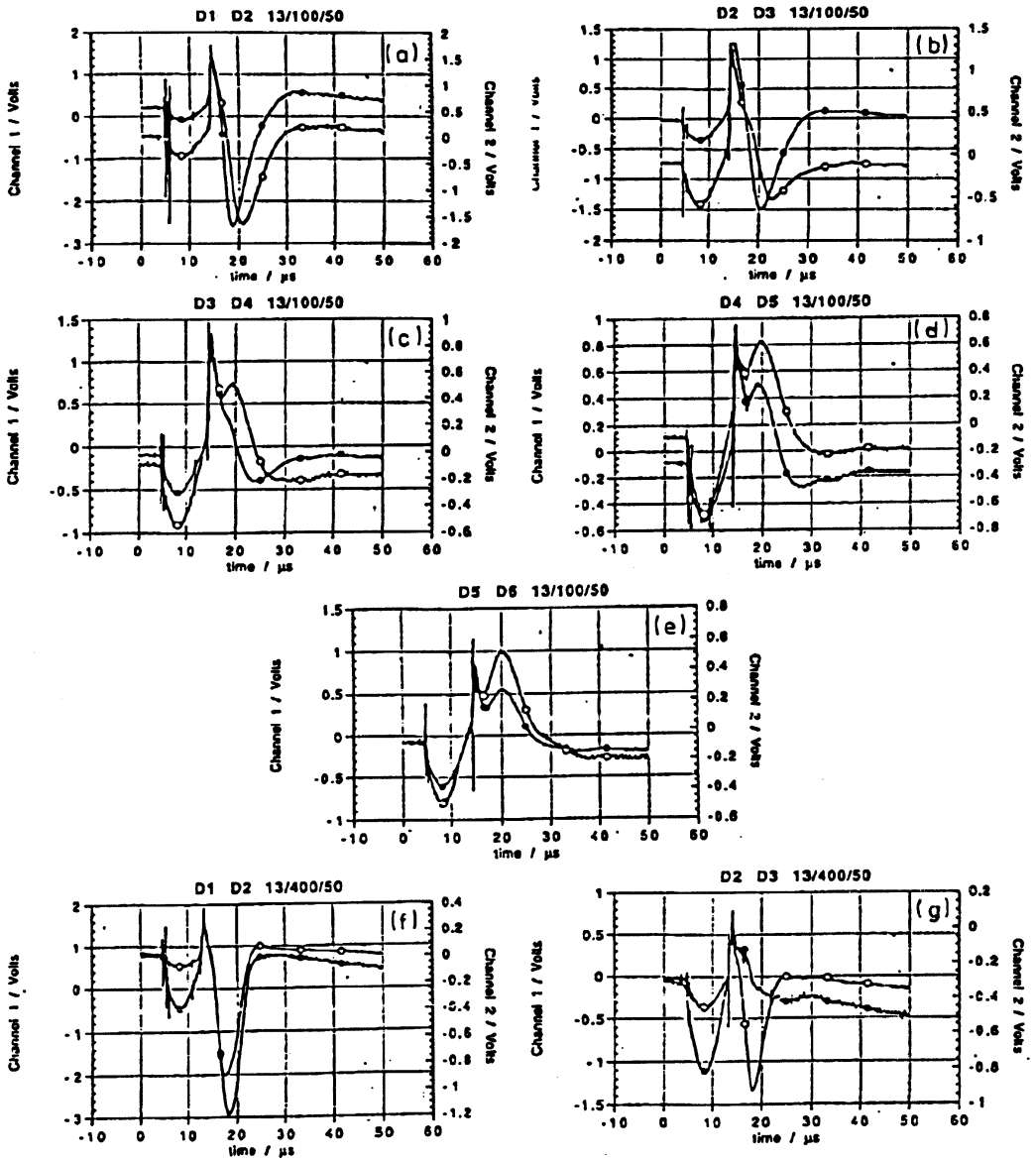

Fig. 19. (a–e) The same series as Fig. 17 b-f, but for helical bias field. The notation is still the same as in Fig. 17 b–f. The explanation of the figures is given in the text. • channel 1, ∘ channel 2; (f) The notation is still the same; the axial field discharge current is here +4000 A. First there seems to be no difference to Fig. 19a; (g) Already at D3 the toroidal current is zero and will be reversed in the following.

The flow of helical currents has been observed previously by others, in some cases, the helical current had the form of a helical pinch exiting from the central electrode [7]. But in that case, each probe should measure the same time of occurrence of the positive pulse after triggering. And furthermore, in Fig. 19a the ratio of the time of occurrence of the pulse amplitudes of the negative and the positive pulse should be $(f+1)/f = 1.33$, since the shock speed equals $(f+1)/f$ times the sheet speed. This is exactly what is observed, in Fig. 19a the ratio is 1.3, and throughout Fig. 19 the positive pulse occurs at the same time. It is observed that the toroidal current decays more rapidly, because of the penetration into the strong field region. Eventually, the toroidal current seems to be reversed. This is due to the resulting Lorentz force of the configuration. If the field polarity was reversed, one expects that the toroidal current, and therefore the flux

is amplified[11]. But upon changing the field polarity, the electron cloud effect again took place, so that no toroidal current was measured (because of a bad breakdown). This is also the explanation of why the optimum field is 3 times less than the computed value. According to the computation, the current in the coil should be 3 kA. But then, toroidal current reversal occurs too fast, leading to very fast instabilities and disruptions, finally to extinction (Fig. 19 f, g). Thus the field has to be less, so that the current reversal is slow. The initial decay actually aids the stability, since the q value increases. So there is still an approximate agreement, if the reversal is not a primary consideration. In the case without quasi-tokamak geometry, the toroidal current goes to zero and becomes extinct; in the present case, the current goes through zero, but then rises again to further heat and stabilize the plasma, i.e. the lifetime is greatly enhanced. This is seen readily from Fig. 17 b–f (toroidal), respectively 19 a–e (helical). In the latter case, there is toroidal current for much longer, with a considerable amplitude. From D6 up to D9 (end of drift space), the signal form remained essentially constant, except for the minute delays, which means a lifetime enhancement of approximately a factor 3 of the plasma in general. Note though that after reversal, there is a superposed helical discharge to the moving plasma, i.e. one can no longer talk of a well defined torus (synchronous positive pulses). If the complex field geometry with its disturbing effects allowed a synchronization in order to achieve flux amplification, the rings would even have longer lifetimes. Experimentally though, it will be difficult to get rid of problems of the kind of bad breakdown at the muzzle. The magnetic diagnostics give the same conclusion as in the previous section: the toroidal current again is very homogeneous and decays continuously, not abruptly. No oscillatory instabilities occurred. If the stabilizing effect of the magnetic field in particular is to be studied in depth, one might think that it would be better to operate the gun with a gas puff, since the stabilizing effect of the rarefaction wave pattern is considerable. But then, there are mechanical torus oscillations when the plasma is ejected until it relaxes to equilibrium, similar to those encountered in a theta-pinch [41]. Thus overall, the high density regime with quasi-tokamak geometry is advantageous.

4.5. Variation of parameters

The optimum discharge voltage was determined to be 13 kV. If the potential was risen above that, breakdown occurred right on the beginning of the first half-period, often resulting in much noise and non-reproducible pulses due to inhomogeneous breakdowns. When the voltage was reduced to 8 kV, not much plasma mass left the gun, or no plasma discharge took place at all. The pressure was varied within 10 mTr to 200 mTr, but only in the region of 20 mTr to 70 mTr a toroidal current was measured. Above 70 mTr, breakdown again is affected, so that pulses become much noisier and are less reproducible. Furthermore, the resistance of the plasma becomes higher, so that the toroidal current decays much faster. For the sheet speed the model predicts: $u_z \sim p^{-1/2}$, this was observed and is shown in Fig. 20 (consider its legend). The author would have liked to do a mapping at different t, in order to show the agreement of the model with the experiment over a wider parameter range. But experimentally, there seems to be a very narrow parameter domain, in which the gun works properly. Actually, this domain can be computed using the model. There seems to be a low and high pressure cutoff, the narrow operation region lying in between. There is also a problem with the breakdown. For example, if the pressure is low, say 30 mTr, the ignition point is no longer precisely defined at the breech, it can also occur in the middle of the gun. But then the sheet speed is uncontrollably affected, i.e. the model is no longer satisfactory, since it assumes a known acceleration

[11] Where the energy is supplied from the axial bias field.

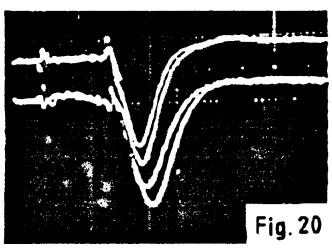

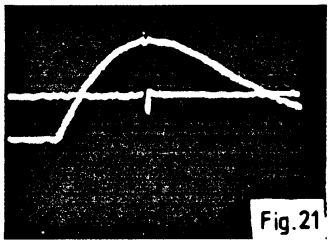

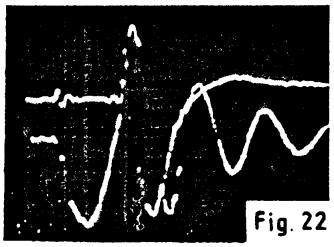

Fig. 20. Picture from the oscilloscope; from top to bottom trace: D1, D2 (60 mTr), D1, D2 (40 mTr), where the deflection is 0.2 V/div, 5 μs/div, 12 kV. According to the model, the ratio of the two time delays should be 0.81, to which the measured ratio of 0.78 is in agreement.

Fig. 21. Timing of the two discharges. Upper trace: plasma discharge current; lower trace: axial field coil discharge current. The sensitivities of the traces have been selected in such a way that the signals can be viewed clearly.

Fig. 22. Plasma discharge current and signal of D1. Upper trace D1 (0.5 V/div); lower trace: plasma discharge current (uncalibrated). 5 μs/div, 60 mTr, 12 kV. The first half-period is longer since the current flows through the central conductor.

length. Generally, the lower the pressure, the higher the probability that breakdown does not occur at the very breech. The axial magnetic field was varied between 0.065 T and 0.26 T (max. flat-top values). If the pressure is risen above 60 mTr, the probability for single-spark discharges in the gun rises, recognizable by spikes in the Rogowski signal of the total discharge current. Evidently, the model then is no longer suitable, for similar reasons as in the low pressure cutoff. It was observed that the stronger the field the faster the toroidal current was reversed, because of the resulting Lorentz force. This still is a stability enhancement, since the current is not extincted when passing zero. Synchronization was impossible to achieve, as discussed in Sec. 4.4. Figure 21 shows the timing of the two discharges, whereas Fig. 22 shows the discharge current on the same time scale along with the signal from the first diamagnetical probe.

5. Conclusion

The modified design in the high density regime was investigated with the conclusion that a CPG can be built much less complicated than previous devices. Especially the central conductor of the inner electrode proved to be rather useful, since it (1) provides the toroidal bias field, (2) causes second half-period breakdown allowing autopreionization, and (3) aids the diagnostics. These results readily are a design improvement. The rather important innovation is the achievement of tokamak field geometry in a CPG, where the stability was enhanced by a factor of approximately 3. The rarefaction wave pattern of the supersonic flow at the muzzle also aids the stability enhancement. The MHD current element model based on the snowplow theory and the Hugoniot–Rankine relations is in very good agreement with experimental data, analytical solutions, i.e. "ready-to-plug-in" equations have been obtained, which can easily be used for other guns in the high density regime. The model furthermore explains the velocity limitation in a very simple way, and the diffusion can be neglected (which might not be true for different operation parameters). It was observed that there seems to be a rather narrow parameter domain if the gun has to work properly, in particular, there seem to be steep pressure cutoffs. Also of considerable importance is the sensitivity of the breakdown to magnetic fields, a problem that will always be encountered in future experiments which might even have

more complicated geometries. The present results are, among other application domains, of importance to future magnetic confinement injection devices, especially for spheromaks.

Acknowledgments

I am greatly indebted to my mentor Dr. R. Keller, who is the retired director of CRPP. Without him this work would never have existed. I am also very indebted to the Centre de Recherches en Physique des Plasmas (CRPP) of the Swiss Federal Institute of Technology in Lausanne (Switzerland), since they allowed me to carry out the project in their laboratory facilities and to use their equipment for my apparatus (I was still a secondary school student). I thank my principal and teachers for their understanding and numerous dispensations from classes they had to issue making it possible for me to go to the laboratory at CRPP in Lausanne. Thanks also to ATEL Inc. in Olten, who took care of the sponsoring for the parts to be manufactured and general expenses by a very generous research grant. Finally, I thank my family for their support.

References

[1] J. Marshall, in: *Proc. Second United Nations Conf. on the Peaceful Uses of Atomic Energy*, Vol. 31, United Nations, Geneva 1958, p. 341

[2] H. Alfvén, in Ref. [1], p. 3

[3] J. Marshall, *Phys. Fluids* **3**, 134 (1960)

[4] H. Alfvén, L. Lindberg, P. Mitlid, *J. Nucl. Energy C* **1**, 116 (1960)

[5] C.T. Chang, *Phys. Fluids* **4**, 1085 (1961)

[6] D.M. Wetstone, *Phys. Fluids* **5**, 981 (1962)

[7] L. Lindberg, C.T. Jacobsen, *Phys. Fluids Supp.* **7**, S44 (1964)

[8] J.W. Mather, *Phys. Fluids Supp.* **7**, S28 (1964)

[9] D.M. Wetstone, I. Greber, *Phys. Fluids Supp.* **7**, S35 (1964)

[10] C.J. Michels, P. Ramins, *Phys. Fluids Supp.* **7**, S71 (1964)

[11] G. Hergizer, H. Krompholz, W. Schneider, K. Schönbach, *Phys. Lett. A* **71**, 54 (1979)

[12] Yu.V. Skvortsov, *Phys. Fluids B* **4**, (1992)

[13] D. Dietz, *J. Appl. Phys.* **62**, 2669 (1987)

[14] P.K. Browning, G. Cunningham, et al., *Phys. Rev. Lett.* **68**, 1722 (1992)

[15] D.G. Swanson, R.W. Clark, P. Korn, S. Robertson, C.B. Wharton, *Phys. Rev. Lett.* **28**, 1015 (1972)

[16] D.C. Hagerman, J.E. Osher, *Phys. Fluids* **4**, (1961)

[17] T.K. Fowler, F.H. Coensgen, in T.K. Fowler, *Mirror Machine Research*, p. 299

[18] R.A. Dory, D.W. Kerst, et al., *Phys. Fluids* **9**, 997 (1966)

[19] A.W. Leonard, R.N. Dexter, J.C. Sprott, *Phys. Fluids* **30**, 2877 (1987)

[20] D.J. Hoffman, J.N. Talmadge, J.L. Shohet, *Nucl. Fusion* **21**, 1130 (1981)

[21] P.K. Browning, G. Cunningham, et al., in: *Physics of Alternative Confinement Schemes, ISPP-8 "Piero Caldirola"*, Eds. S. Ortolani, E. Sindoni, SIF, Bologna 1991, p. 1047

[22] J. Marshall, T.F. Stratton, *Nucl. Fusion Supp.* Part 2, 663 (1962)

[23] N.H. Kemp, H.E. Petschek, *Phys. Fluids* **2**, 599 (1959)

[24] Mei-Yu Wang, C.K. Choi, F.B. Mead Jr., *AIP Conf. Proc.* **246**, 30 (1992)

[25] T. Ikehata, K. Oohashi, et al., *Nucl. Instrum. Methods Phys. Res. B* **70**, 26 (1992)

[26] C. Kim, D.F. Ogletree, *Appl. Surf. Sci.* **59**, 261 (1992)

[27] S.K. Iyyengar, V.K. Rohatgi, in *1989 Int. Conf. on Plasma Physics*, Vol. 3, p. 1165

[28] K.H. Kwek, T.Y. Tou, S. Lee, *IEEE Trans. Plasma Sci.* **18**, 826 (1990)

[29] M. Rosenbluth, R. Garwin, A. Rosenbluth, *U.S. Atomic Energy Comission*, Report LA-1850, 1954

[30] J. Keck, *Phys. Fluids Supp.* **7**, S16 (1964)

[31] L.C. Burkhardt, R.H Loveberg, *Phys. Fluids* **5**, 341 (1962)

[32] D.J. Rose, M. Clark Jr., *Plasmas and Controlled Fusion*, M.I.T. Press, 1961

[33] L. Spitzer, *Physics of Fully Ionized Gases*, Interscience, New York 1956

[34] R. Courant, K.O. Friedrichs, *Supersonic Flow and Shock Waves*, Interscience, New York 1961

[35] K. Thom, J. Norwood, N. Jalufka, *Phys. Fluids Supp.* **7**, S67 (1964)

[36] V.D. Shafranov, V.S. Mukhovatov, *Nucl. Fusion* **11**, 605 (1971)

[37] J. Wesson, *Tokamaks, Oxford Engineering Science Series — 20*, Clarendon Press, 1987

[38] Om P. Gandhi, *Microwave Engineering and Applications*, Pergamon Press 1986

[39] S. Schaer, CRPP/ Ecole Polytechnique Fédéral de Lausanne, LRP 491/94, 1994

[40] S. Schaer, *Helv. Phys. Acta* **67**, 217 (1994)